



Caustics of the axially symmetric vortex beams: analysis and engineering

Na Xiao, Chen Xie, François Courvoisier, Minglie Hu

► To cite this version:

Na Xiao, Chen Xie, François Courvoisier, Minglie Hu. Caustics of the axially symmetric vortex beams: analysis and engineering. Optics Express, 2022, 30 (16), pp.29507-29517. <hal-03831660>

HAL Id: hal-03831660

<https://hal.science/hal-03831660v1>

Submitted on 27 Oct 2022

HAL is a multi-disciplinary open access archive for the deposit and dissemination of scientific research documents, whether they are published or not. The documents may come from teaching and research institutions in France or abroad, or from public or private research centers.

L'archive ouverte pluridisciplinaire **HAL**, est destinée au dépôt et à la diffusion de documents scientifiques de niveau recherche, publiés ou non, émanant des établissements d'enseignement et de recherche français ou étrangers, des laboratoires publics ou privés.



HAL Authorization

Caustics of the Axially Symmetric Vortex Beams: Analysis and Engineering

NA XIAO,¹ CHEN XIE,^{1,*} FRANÇOIS COURVOISIER,² AND MINGLIE HU¹

¹Ultrafast Laser Laboratory, Key Laboratory of Opto-electronic Information Science and Technology of Ministry of Education, College of Precision Instruments and Opto-electronics Engineering, Tianjin University, 300072 Tianjin, China

²FEMTO-ST Institute, Université de Bourgogne-Franche-Comté UMR-6174, 25030 Besancon, France

*xie_chen@tju.edu.cn

Abstract: We demonstrate that our theoretical scheme developed in the previous study on the caustics of the abruptly autofocusing vortex beams [Xiao *et al.*, Opt. Express **29** (13): 19975 (2021)] is universal for all the *axially symmetric vortex beams*. Further analyses based on this method show the complex compositions of the vortex caustics in real space. Fine features of the global caustics are well reproduced, including their deviations from the trajectories of the host beams. Besides, we also show the possibility of tailoring the vortex caustics in paraxial optics based on our theory. The excellent agreements of our theoretical results with both numerical and experimental results confirm the validity of this scheme.

© 2022 Optica Publishing Group under the terms of the Optica Publishing Group Open Access Publishing Agreement

1. Introduction

Vortex beams are structured light fields with doughnut-shaped spatial profiles and phase singularities. Their distinctive feature is the presence of the helical phase fronts described as $\exp(i l \theta)$, where l is the so-called topological charge and θ is the azimuthal angle [1]. Among the vortex beams, the spiral vortex beams are shown to be strong in terms of the structural stability [2,3]. Due to these notable properties, vortex beams have attracted widespread interests and play critical roles in various applications, like particle micromanipulation [4,5], microscopy [6], material processing [7-9], and optical communication [10,11]. By superimposing the helical phase on the axially symmetric phases of different host beams like the Gaussian beam, the Bessel beam and the abruptly autofocusing beam, a series of axially symmetric vortex beams (ASVBs) are investigated [12-15]. In this way, vortex beams can be adapted with diverse intensity tubes in focusing, diverging and non-diffracting shapes.

Two major schemes are basically implemented to interpret and engineer the light fields. The integral-based scheme is the mostly-used method, involving with the diffraction integral using the stationary phase method [16-19]. In some cases, the use of this method induces “singular points” whose intensity tends to infinity [20]. Various asymptotic methods have also been discussed to analyze the field around the irremovable singular points [20-23]. As the approximation is indispensable to simplify the diffraction integral, error estimates as well as complex algebra are required. In parallel, the differentiation-based scheme is also developed in the realm of the geometric optics. In this scheme, vortex light fields can be decomposed into families of rays emerging from any cross-section along propagation [24,25]. And the envelope of the ensemble of rays constitutes the framework of the caustics [24, 26]. In this way, a relatively simple and efficient method without further approximation is available to interpret the caustics of ASVBs and to predict the focusing properties in real space [27]. However, some clarifications of the compositions of caustics in real space have not been discussed. In addition, for applications like microscopy, laser ablation and fabrication of two-photon polymerization, tailoring the caustics have also been an increasing interest in recent years [28-32]. With a

comprehensive understanding of the caustics, engineering the caustics of the ASVBs is also an issue of fundamental importance in applications.

In this paper, we show a developed approach to classify the caustics of different ASVBs. In Section 2, we firstly introduce the theoretical results as a set of concise expressions developed for reproducing the caustics of the ASVBs. Comparing with the existing results, these expressions are obtained without any mathematical approximation. Then, the third Section compares our theories with the numerical simulations and the experimental results for several exemplary beams, illustrating the geometries of the vortex caustics. In particular, finer features can be well outlined in more intuitive physical images as shown in the discussion of the Bessel vortex beam and the abruptly autofocusing vortex beam, which are absent in previous studies. Furthermore, we also developed a method to engineer vortex beams with tailored novel tubular caustics based on our results. Our theoretical results are in excellent agreement with both numerical simulations and experimental results.

2. The caustics of the ASVBs

2.1 Analytical results

From a given *axially symmetric* host beam with the phase profile $\phi_{\text{host}}(r)$, the vortex version can be synthesized by combining the spiral phase $\phi_{\text{vortex}}(\theta) = l\theta$ with $\phi_{\text{host}}(r)$ in any cross-section along propagation [27]:

$$\phi(r, \theta) = \phi_{\text{host}}(r) + \phi_{\text{vortex}}(\theta) = \phi_{\text{host}}(r) + l\theta \quad (1)$$

In geometrical optics, the corresponding radial components of the k vector can be defined as $k \cdot \sin \gamma(r) \equiv -\partial \phi(r, \theta) / \partial r = -\partial \phi_{\text{host}} / \partial r$, where $k = 2\pi/\lambda$ is the wave number depending on the wavelength λ [27]. Note that this angle is only related to the host beam. With the parameters N and V defined as:

$$N(r) = \sqrt{\sin^2 \gamma + l^2 / (kr)^2} \quad (2)$$

$$V(r) = \sqrt{N^2 - 1}$$

we found that the rays emerging from the ring of a specific radius r in the initial transverse plane $z = 0$ lie on the hyperboloid [Fig. 1(a)] specified as:

$$\frac{\rho^2}{R^2} - \frac{(z - z_w)^2}{L^2} = 1 \quad \rho^2 = x^2 + y^2 \quad (3)$$

$$R = \frac{|l|/k}{N}, \quad L = RV, \quad z_w = \frac{V}{N} \sqrt{r^2 N^2 - \frac{l^2}{k^2}}$$

where R , L and z_w are all dependent on r for a given topological charge l . Moreover, the whole light field can be represented in geometrical optics as the superposition of ray families lying on different hyperboloids [Fig. 1(b)], leading to their envelope defined as the caustic of the synthesized vortex beam from the host field. Here we postulate the existence of the caustic, and we found that the z positions of the *constituent* points on the caustic (or the *characteristic* points in [27]) are simply the solutions to the equation:

79

$$A(z - z_w)^2 + B(z - z_w) + C = 0$$

80

$$A = (LVN)^{-2} \frac{R'}{R}, \quad B = \frac{z_w'}{L^2}, \quad C = -\frac{R'}{R} \quad (4)$$

$$\Delta \equiv \sqrt{B^2 - 4AC}$$

81

where the prime denotes a derivative with r . Since the Eq. (4) is quadratic, there are two sets of *constituent* points $(\rho(z_1), z_1)$ and $(\rho(z_2), z_2)$ for each given parameter r :

82

83

$$z_1 = z_w - \frac{B - \Delta}{2A}$$

$$z_2 = z_w - \frac{B + \Delta}{2A} \quad (5)$$

84

Note that the host phase $\phi_{\text{host}}(r)$ is represented by the specific distribution of $\sin \gamma(r)$ through differentiation. And the introduction of the parameters N and V in Eq. (2) can further facilitate the understanding on the geometrical image of the vortex beams. One can easily calculate the complex caustic by substituting (N, V) of a specific host phase into Eqs. (3) - (5). Since no integral is involved in this procedure, our differentiation-based method is very friendly to implement without further approximations.

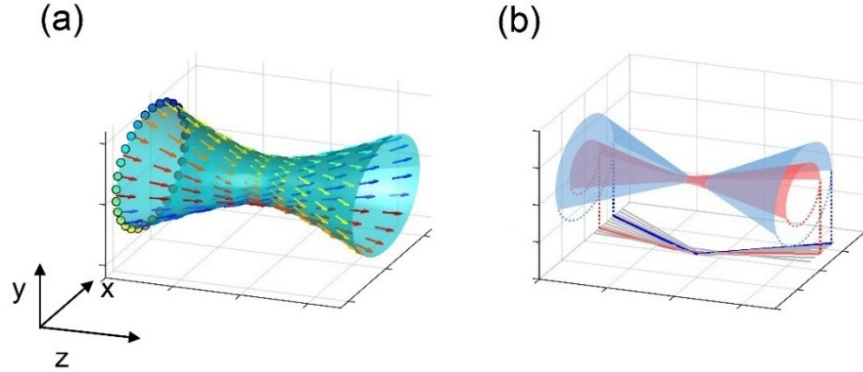
85

86

87

88

89



90

91

92

93

94

95

96

Fig. 1. Schematics of the axially symmetric vortex beams (ASVBs) in geometrical optics: (a) a single hyperboloid formed by rays emerging from a specific ring in the transverse plane $z=0$; (b) Two different hyperboloids formed by the corresponding families of rays from the plane $z=0$ (the blue and red half tubes), with their intersections with $y=0$ plane (blue and red solid curves) projected into the bottom plane. The intersections between other hyperboloids and $y=0$ plane are also superimposed (gray solid curves). The whole beam propagates in the z direction.

97

2.2 Discussions on the topology of the caustics

98

In this work, we focus on the caustics in *real* space of an optical setup ($z > 0$) since the beam is usually generated in such ways. In general, the *constituent* points of the global caustics of the ASVBs can be rather complex: *either* a single set of $\{z_1\}$ (or $\{z_2\}$) *or* both sets of $\{z_1\}$ and $\{z_2\}$ can get involved in constituting the caustic in real space (as will be shown in Section 3.2). After some algebra, we find that the expression below can well distinguish the above two general cases in terms of z_w :

100

101

102

103

$$\begin{aligned}
\text{Both sets: } z_w &> \frac{B + \Delta \cdot \text{sgn}(R')}{2A}, \quad z_1 > 0, z_2 > 0 \\
\text{Single set: } z_w &< \frac{B + \Delta \cdot \text{sgn}(R')}{2A}, \quad z_2 < 0 < z_1 \text{ (or } z_1 < 0 < z_2)
\end{aligned} \tag{6}$$

where $\text{sgn}(R')$ is the sign function. Besides, the relative locations of z_1 and z_2 for a specific host beam are determined by R' . More details of the cases are summarized in Table 1.

Table 1. Constituent points in real space ($z > 0$)

No. of solution sets	Two sets: $\{z_1\}$ and $\{z_2\}$	A single set: $\{z_1\}$ (or $\{z_2\}$)
Sign of R'		
+	$0 < z_2 < z_1$	$z_2 < 0 < z_1$
-	$0 < z_1 < z_2$	$z_1 < 0 < z_2$

3. Numerical and experimental demonstration of the caustics of different ASBVs

3.1 Setup

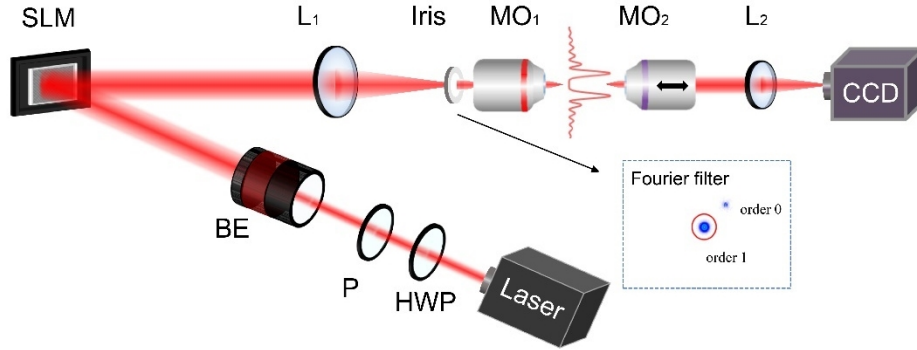


Fig. 2. Schematic of the experimental setup. HWP: half-wave plate; P: polarizer; BE: beam expander; SLM: spatial light modulator; L: lenses; MO1 and MO2: microscope objectives.

We use the same setup as in [27] to demonstrate our analytical results in section 2. As shown in Fig. 2, the Gaussian beam centered at 1065nm from a home-made ultrafast fiber laser is firstly injected into a beam expander. The output collimated beam with an expanded width of ~8mm is then incident upon a phase-only spatial light modulator (Holoeye SLM-Pluto, 1920×1080 pixels). The exposed power is controlled by adjusting the half-wave plate before a polarizer. With the phases of the synthesized vortex beams in Table 2 encoded on the SLM together with an additional grating phase, ASBVs can be generated right after SLM in the first order. Then a telescope is used to shrink the ASBVs down to the micron-scale. The telescope is built with a lens (focal length = 1m) and a microscope objective (50×, NA = 0.8). An iris is installed close to MO₁ to block the undesired orders, retaining the first order of the diffraction lights as shown in the inset of Fig. 2. An imaging system made of another identical microscope objective (MO₂) followed by a lens (focal length = 0.5m) is used to capture the intensity profiles at each z position along beam propagation. The 2D side views of the intensity profiles are then

extracted from the stacked data. Careful alignments only introduce weak perturbation in the setup. This guarantees that the vortex beams appear with negligible deviation from the ideal caustics.

3.2 Experimental demonstrations

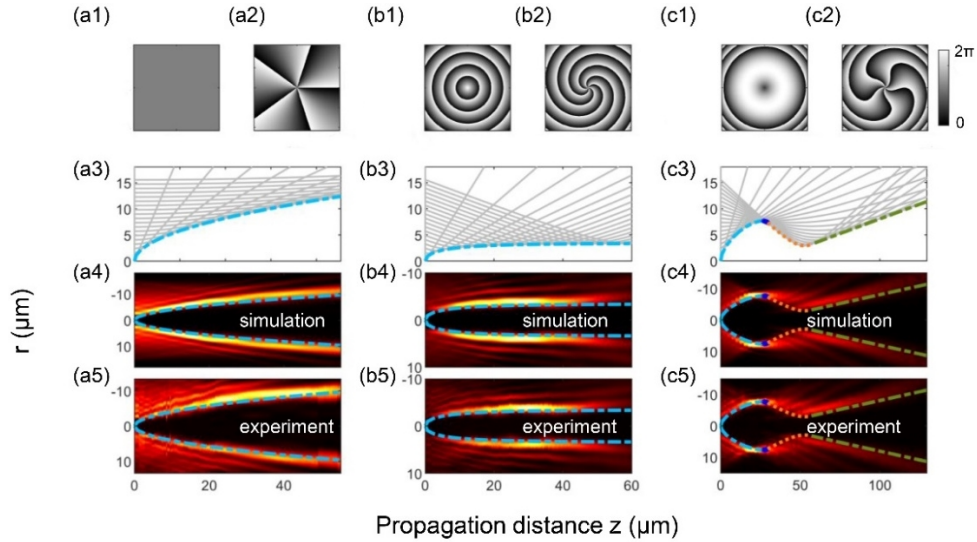
In our previous study on vortex beams hosted by the abruptly autofocusing beams [27], it is proved that the caustics of their central tube can be well described by the set of constituent points determined by Eq. (3)-(5). To further demonstrate the universality of our formulae for the whole family of axially symmetric vortex beams (ASVBs), vortex beams with four additional host beams, such as Gaussian beams, Bessel beams, Bessel-like beams [33] and parabolic toroidal lens beams [34] are generated in this work. Table 2 lists their phases and the corresponding $\sin \gamma(r)$.

Table 2. Phases of four vortex beams synthesized from specific host beams

Specific ASVBs	Applied phase and their $\sin \gamma(r)$: caustics of two simplest cases are given in the parentheses
Gaussian vortex beam	$\phi(r, \theta) = l\theta$ $\sin \gamma(r) = 0$ $\left(z = \frac{\rho^2 - (l/k)^2}{2 l/k } \right)$
Bessel vortex beam	$\phi(r, \theta) = -k \sin \gamma \cdot r + l\theta$ $\sin \gamma(r) = \text{constant}$ $\left(z = \frac{\rho^2 \sin \gamma}{ l/k } \sqrt{\frac{\rho^2 - (l/k)^2}{(l/k)^2 - \rho^2 \sin^2 \gamma}} \right)$
Bessel-like vortex beam [33]	$\phi(r, \theta) = -k(ar^n + br^m) + l\theta$ $\sin \gamma(r) = nar^{n-1} + mbr^{m-1}$
Parabolic vortex toroidal lens [34]	$\phi(r, \theta) = -k(r^2 - 2r_0 r)/2f + l\theta$ $\sin \gamma(r) \equiv (r - r_0)/f$

According to section 2, the caustics of the ASVBs with a given topological charge l are only related to the corresponding host phases. Without loss of generality, the topological charge l is chosen to be $l = 5$ for this section. Based on the angular spectrum method [35], we also numerically simulate different ASVBs with parameters corresponding to the setup in Fig. 2. The simulated and experimental results are shown in Fig. 3, where the measured 2D intensity profiles are extracted from the 3D data acquired with our setup. For Gaussian vortex beams, the phase of the host Gaussian beam as well as the corresponding total phase of the ASVB are shown in Fig. 3(a1) - (a2). The flat phase of the host Gaussian beam results in $z_w = 0$ and $B = 0$ for any r , which gives $z_2 = -z_1$ with $z_1 > 0$. According to Table 1, the caustic in real space is determined only by the single set of z_1 , shown by the blue dash-dotted line in Fig. 3(a3) - (a5). In the second example, the phases of the host Bessel beam with $\sin \gamma(r) \equiv 8.87 \times 10^{-4}$ and the corresponding vortex beam are shown in Fig. 3(b1) - (b2). As Bessel vortex beam determines that $R'(r) > 0$ and $z_w < (B + \Delta)/2A$, the sign of z_1 and z_2 can be solved as $z_1 > 0$ and $z_2 < 0$. In this way, the caustic in real space is also determined by the single set of z_1 as shown in Fig. 3(b3) - (b5) with the blue dash-dotted line. Besides, the set of $(\rho(z_1), z_1)$ can be well approximated by the set of $(R(r), z_w(r))$ for Bessel vortex beams. Comparing with the cylindrical caustic expected for Bessel vortex beams [23], our solution in Table 2 can well outline the finer features of the transitionally-expanding tube caustic as shown in [25]. The cylindrical caustic is the special case where the approximation $l/(kr) \ll \sin \gamma$ is applied in the expression $R(r)$ in Eq. (3). We stress here that the analytical results in this paper also address the puzzling correspondence between the ensemble of the hyperboloidal waists and the central tube caustics of Bessel vortex beams in our previous study [25].

164 A family of perfect optical vortices (POVs) are recently designed by integrating the spiral
 165 phase into the phase of the parabolic toroidal lens [34]. This POV with a large range of
 166 topological charge l has a quasi-static focal ring radius r_0 at a focal length f . The set of equations
 167 determining the caustics of these beams are too complex in [34], resulting in analytical
 168 estimates in two special cases. Since our analytical results are deduced for any axially
 169 symmetric vortex beam without any further estimate, we also generate one of such beams to
 170 demonstrate the validity of our method. The corresponding beam parameters after the telescope
 171 in Table 2 are selected as $f = 30\mu\text{m}$ and $r_0 = 7\mu\text{m}$. After some algebra, we found the caustic of
 172 this specific POV can be decomposed into multiple sections. When a given r is small enough
 173 that $z_w(r) < [B + \Delta \cdot \text{sgn}(R')] / 2A$ and $R' > 0$, the single set of $z_l(r)$ define the most front section of
 174 the caustic [the blue dash-dotted line in Fig. 3(c3)–(c5)]. As r grows until $z_w(r) > [B + \Delta \cdot \text{sgn}(R')] / 2A$,
 175 both the solution sets in Eq. (5) are involved in forming the caustic: $\{(\rho(z_1), z_1(r))\}$ define
 176 a tiny part of the caustic very close to the original focal plane of the host beam [dark blue lines
 177 in Fig. 3(c3)–(c5)]; $\{(\rho(z_2), z_2(r))\}$ determine the long opening tube behind, as shown by the
 178 green dash-dotted line in Fig. 3(c3)–(c5). The intermediate caustic section [orange dots] in the
 179 range of $[z_1(r_{\max}), z_2(r_{\max})]$ between the short dark blue line and the green line is composed by
 180 part of the hyperboloid formed by the rays emerging from the edge of the effective aperture.
 181 Besides, when the vortex order is increased, the section $\{(\rho(z_1), z_1(r))\}$ before the focus remains
 182 quasi-static and the section $\{(\rho(z_2), z_2(r))\}$ after the focus is shorter. In short, the complex global
 183 caustics can be well analyzed with our method. Our analytical results are in excellent agreement
 184 with both numerical simulation and experimental results.



185
 186 Fig. 3. The results of different ASVBs with topological charge $l = 5$. (1)–(2): The phases of the
 187 host beams and the corresponding ASVBs. (3)–(5): The theoretical, numerical and experimental
 188 results for (a) Gaussian vortex beam, (b) Bessel vortex beam and (c) perfect optical vortex beam
 189 generated by parabolic vortex toroidal lens. Light blue dash-dot lines together with dark blue
 190 short lines represent the caustic defined by $(\rho(z_1), z_1)$. Green dash-dot lines represent the caustic
 191 defined by $(\rho(z_2), z_2)$. Orange dot lines represent part of the caustic formed by part of the
 192 hyperboloidal surface between $(\rho(z_1), z_1)$ and $(\rho(z_2), z_2)$ occurred in the perfect optical vortex.

193 In addition, our results can well reproduce the deviation of the propagating behavior of the
 194 synthesized vortex beam from that of the corresponding host beam with specific parameters.
 195 The topological charge l is also chosen to be $l = 5$. Here, we firstly selected the Bessel-like
 196 beam in [33], *i.e.* a family of shape invariant beams, as the host beam. For specific Bessel-like
 197 beams with a linearly ramped central lobe along propagation, the parameters are selected as n
 198 $= 2$, $m = 1$ in Table 2. As for the Bessel-like beams featuring the linearly diverging central lobe,

the parameters are chosen as $a = -0.17 \text{ m}^{-1}$, $b = 0.0018$. With $R' > 0$ and $z_w < (B+\Delta)/2A$, z_2 is negative. Therefore, the global caustic is also defined by the single set of z_1 , shown as the blue dash-dot lines in Fig. 4(a). For comparison, the central lobe profile of the Bessel-like beam without the spiral phase is superimposed as the purple line in Fig. 4(a3). It is evident that the spiral phase further accelerates the divergence along propagation. In the second Bessel-like beam [shown in Fig. 4(b)], we select the parameters as $a = 0.056 \text{ m}^{-1}$ and $b = 0.0006$ without changing n and m . Instead, this Bessel-like host beam has a linearly-tapered central lobe along propagation, presented by the purple line in Fig. 4(b3). Interestingly, the corresponding ASVB has an extremum on the ring caustic [shown by the single red circle in Fig. 4(b3)] determined by $R'(r_{\text{extrema}}) = 0$. This behavior is totally different from the monotonous tapering of central lobe in the host beam along propagation. In fact, this deviation was also observed in our early work on abruptly autofocusing vortex (AAFV) beams hosted by the polynomial phase [27]. For such AAFV beams with specific parameters (for instance, $n = 4$, $a = 0.3 \times 10^{-4} \text{ m}^{-3}$ and $r_0 = 1.08 \text{ mm}$ as in [27]), the sets of z_1 and z_2 are both involved in constituting the global caustics. Besides the significant deviation of the vortex caustics from the host polynomial trajectories [shown by the purple line in Fig. 4(c3)], the introduction of the spiral phase into the host beam also brings the interesting feature: once the local maximum in the waist distribution $R(r)$ exists, an extremum occurs accordingly on the global caustic despite of the original trajectory of the host beam as shown in Fig. 4. In short, the analyses based on our method can exactly reproduce the fine features of the caustic shape. This further demonstrates the validity of our analytical results, serving as a powerful tool for analyzing the vortex beams.

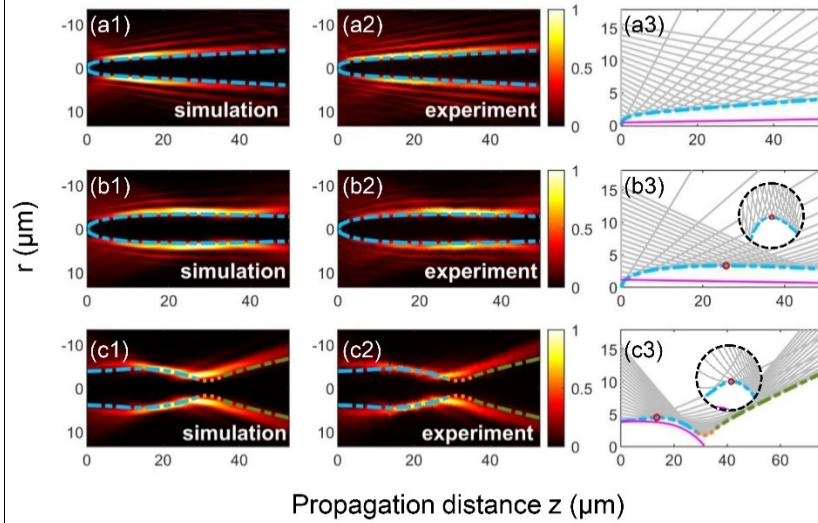


Fig. 4. Propagating behavior deviation of the ASVBs ($l = 5$) from their host beams. Bessel-like vortex beam with parameters: (a) $a = -0.17 \text{ m}^{-1}$, $b = 0.0018$ and (b) $a = 0.056 \text{ m}^{-1}$, $b = 0.0006$; (c) Abruptly autofocusing vortex beams with: $n = 4$, $a = 0.3 \times 10^{-4} \text{ m}^{-3}$ and $r_0 = 1.08 \text{ mm}$. Purple lines in (a3) and (b3) show the central lobe size of the host Bessel-like beam without the spiral phase, and the purple line in (c3) represents the host polynomial trajectory. Blue dash-dot lines represent the caustic defined by $(\rho(z_1), z_1)$ and green dash-dot lines represent the caustic defined by $(\rho(z_2), z_2)$. Orange dot lines in (c1) - (c3) represent part of the caustic formed by part of the hyperboloidal surface between $(\rho(z_1), z_1)$ and $(\rho(z_2), z_2)$ like the perfect optical vortex. Insets of (b3) and (c3) show zoomed extrema points.

4. Engineering the caustics of the ASVBs in the paraxial optics

Previous sections show how to calculate the caustics of the ASVBs from their phases $\phi(r, \theta)$. With the help of the caustic expressions, we also demonstrate that the propagation behavior of

the ASVBs can deviate significantly from that of the corresponding host beams due to the spiral phase. Therefore, a challenge arises here that the host beams cannot always well *predict* the tube shape of their vortex “brother” beams.

In fact, the inverse problem of *tailoring* the caustic by an engineered host phase is more interesting. The target profile $\rho(z) = c(z)$ can be engineered by solving the host phase $\phi_{\text{host}}(r)$ from $z_{\text{caustic}}(r) = c^{-1}(z)$ based on Eq. (4) and (5). However, this usually involves a mathematical challenge. Here, we clarify a fundamental limit and show the possibility of tailoring the tube shape based on our results with two preconditions. Since travelling waves are generated in numerous applications, this leads to a fundamental requirement that the topological charge l should not be very large within the radial contents of the beam, i.e. $|l| \leq kr |\cos \gamma(r)|$. In practice, paraxial optics are adopted in most cases, requiring that $\tan \gamma(r) \approx \sin \gamma(r)$. If we further focus on the ASVBs with the azimuthal components of k vector much smaller than the corresponding radial components, we found $r \gg |l|/\phi'(r, \theta)$ and $\sin^2 \gamma(r) + [l/(kr)]^2 \approx \sin^2 \gamma(r)$. With these preconditions implemented in Eqs. (4) and (5), the tubular caustic can be well approximated as:

$$\begin{aligned} z &\approx r/\tan \gamma \approx r/\sin \gamma = -kr/\phi'_{\text{host}}(r) \\ \rho &= -|l|/\phi'_{\text{host}}(r) \end{aligned} \quad (7)$$

The $\phi_{\text{host}}(r)$ can be solved by substituting the target caustic profiles $\rho(z) = c(z)$ into Eq. (7) with the help of the computer. To demonstrate the validity of our method, several exemplary ASVBs with tailored tubular profiles after the telescope can be generated in our setup. The target profiles and the specific parameters of these beams are listed in Table 3. All the measured caustics present excellent agreements with the corresponding tailored profiles as shown in Fig. 5.

Table 3. Target profiles $\rho(z) = c(z)$ of different shapes

Types of profiles	The target profiles and parameters after the telescope
Quartic	$\rho(z) = a(z - z_0)^4 + b$ $a = 6 \times 10^{12} \text{ m}^{-3}, \quad z_0 = 20 \mu\text{m}, \quad b = 1 \mu\text{m}$
Logarithmic	$\rho(z) = a \log_2(z + b) + c$ $a = 0.2, \quad b = 1 \mu\text{m}, \quad c = 0.5 \mu\text{m}$
Parabolic	$\rho(z) = a(z - z_0)^2 + b$ $a = -9 \times 10^2 \text{ m}^{-1}, \quad z_0 = 50 \mu\text{m}, \quad b = 2.5 \mu\text{m}$
Exponential	$\rho(z) = a \exp[b(z - z_0)] + c$ $a = 1, \quad z_0 = 20 \mu\text{m}, \quad b = 5 \times 10^4 \text{ m}^{-1}, \quad c = 1.5 \mu\text{m}$

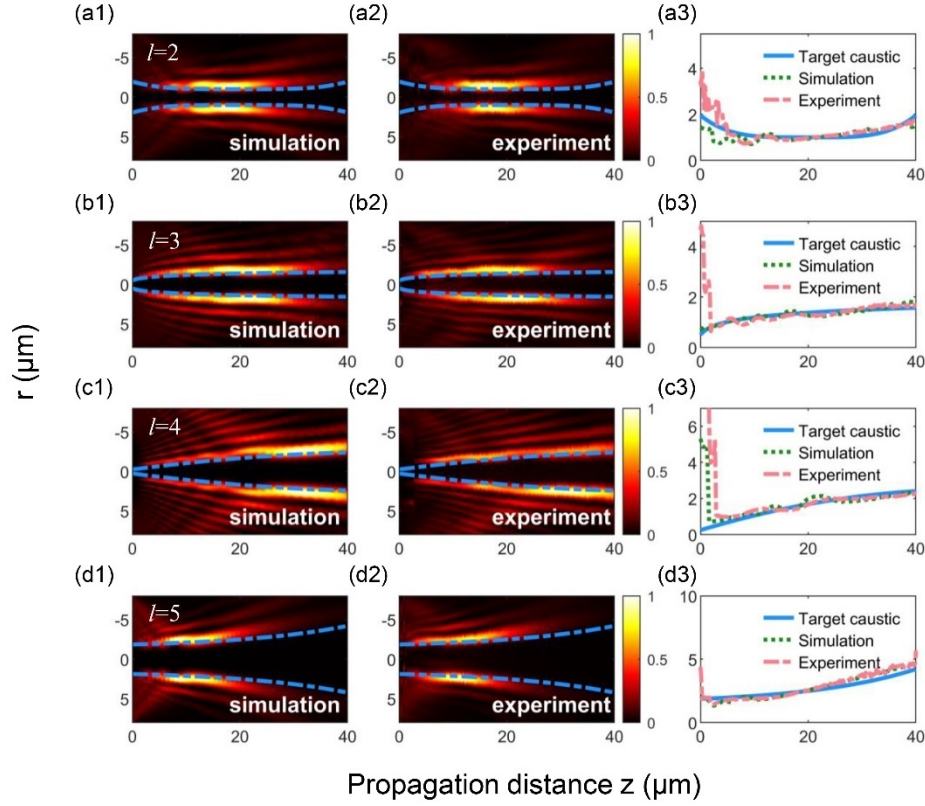


Fig. 5. Synthesized vortex beams of different vortex orders with: (a) quartic, (b) logarithmic, (c) parabolic and (d) exponential tubular profiles and tailored parameters listed in Table 3. The blue dash dotted lines represent the pre-engineered target caustics. The caustic profiles extracted from the simulation and experiments shown in the third column are all defined as in [27].

In addition, two exemplary ASVBs with $l = 6$ are pre-engineered and shown in Fig. 6, presenting one beam carrying an opening central tube profile $\rho(z) = a + bz$ with $a = 2\mu\text{m}$, $b = 0.058$ [Fig. 6(a)] and the other with a tapered central tube profile $\rho(z) = a - bz$ with $a = 5\mu\text{m}$, $b = 0.058$ [Fig. 6(b)]. By inserting Eq. (7) into the above target tube profiles, the engineered phase can be readily obtained as $\phi_{\text{host}}(r) = -(|l/a)r \pm r^2bk/(2a)$. The blue solid lines represent the pre-determined caustics $\rho(z)$. Fig. 6(a3) and Fig. 6(b3) also present the simulated and measured tube profiles. The discrepancies from the target tapered profile in Fig. 6(b) mainly originate from the limited active aperture on the SLM ($8.64\text{mm} \times 8.64\text{mm}$). This is proved by simulating the same beam with SLMs of different areas, where the larger active area ($12\text{mm} \times 12\text{mm}$) allows a better agreement with the predefined geometry [Fig. 6(b5)]. Despite that such a large SLM is unavailable in our experiment, this distortion can be corrected in tailored caustics with a smaller initial ring and a less steep taper ($a = 4\mu\text{m}$, $b = 0.038$) as shown in Fig. 6(c).

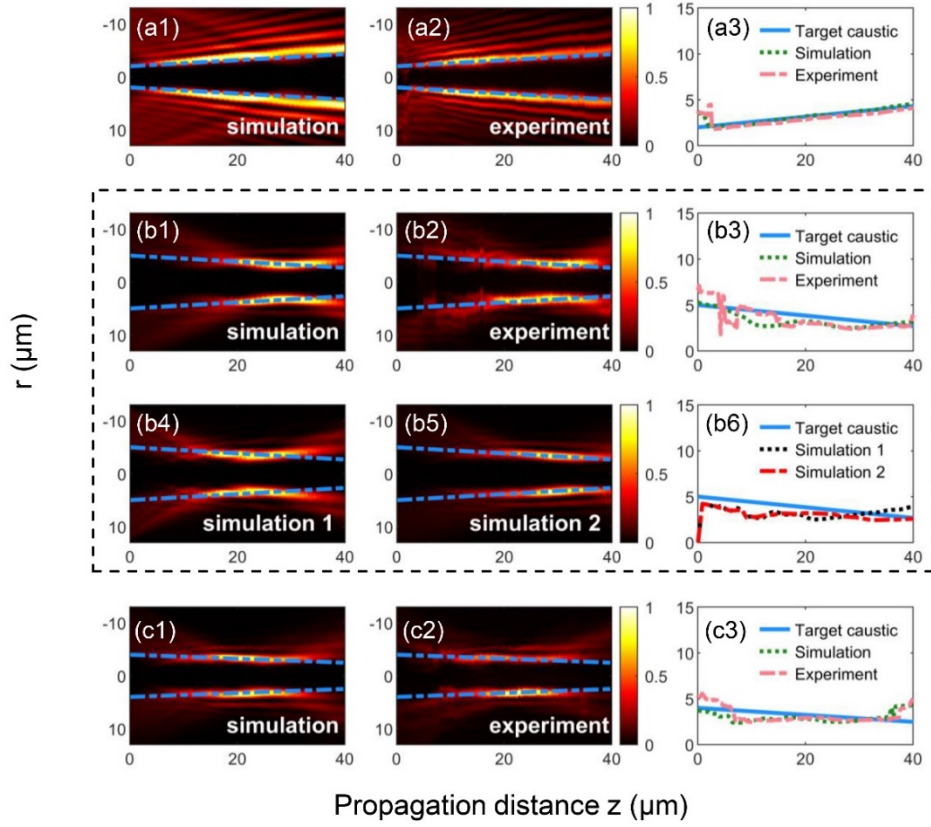


Fig. 6. Numerical simulations and experimental results of several particular examples with the tunable hollow core radius. (a) $\rho = a + bz$ with $a = 2\mu\text{m}$, $b = 0.058$; (b) $\rho = a - bz$ with $a = 5\mu\text{m}$, $b = 0.058$ and (c) $\rho = a - bz$ with $a = 4\mu\text{m}$, $b = 0.038$. SLMs with a smaller ($7\text{mm} \times 7\text{mm}$) and a larger ($12\text{mm} \times 12\text{mm}$) area are adopted in the simulation in (b4) and (b5), respectively. The blue dash dotted lines represent the pre-engineered target caustics. The caustic profiles extracted from the simulation and experiments shown in the third column are all defined as in [27].

5. Conclusion

In this paper, we demonstrate that the set of analytical equations developed in our previous study on the caustics of the abruptly autofocusing vortex beams [27] have a wider universality to well reproduce the caustics of the axially symmetric vortex beams. Based on a couple of vortex beams synthesized from different host beams, the universality is proved by the excellent agreements of our theory with the numerical and experimental results. Features of the vortex caustics can also be well addressed with our theoretical methods, including the components of the global caustics and the deviation of the vortex caustics from the host caustics. Besides, we have also shown that it is possible to pre-engineer the vortex caustics based on our theory in the paraxial regime where the polarization components can be decoupled. Interesting opportunities also arise for extending our work to the nonparaxial regime. We expect that these results will promote the development of numerous applications, such as material processing, microscopy, particle micromanipulation and synthesis of novel electro-magnetic wavepackets [36, 37]. Also, the structural stability of the different solutions in the nonlinear regime can represent interesting future work.

Funding. National Natural Science Foundation of China (61605142, 61827821); Tianjin Research Program of Application Foundation and Advanced Technology of China (17JCJQC43500); Shanghai Institute of Optics and Fine Mechanics, Chinese Academy of Sciences (Open Fund of the State Key Laboratory of High Field Laser Physics); European Research Council (682032-PULSAR); Agence Nationale de la Recherche (ANR-15-IDEX-0003, ANR-17-EURE-0002).

Disclosures. The authors declare no conflicts of interest.

Data availability. Data underlying the results presented in this paper are not publicly available at this time but may be obtained from the authors upon reasonable request.

References

1. L. Allen, M. W. Beijersbergen, R. J. C. Spreeuw, and J. P. Woerdman, "Orbital angular momentum of light and the transformation of Laguerre-Gaussian laser modes," *Phys. Rev. A* **45**(11), 8185–8189 (1992).
2. E. G. Abramochkin, and V. G. Volostnikov, "Spiral light beams," *Phys.-Usp.* **47**, 1177–1203 (2004).
3. A. Volyar and Y. Akimova, "Structural stability of spiral vortex beams to sector perturbations," *Appl. Opt.* **60**(28), 8865–8874 (2021).
4. Y. Yang, Y. Ren, M. Chen, Y. Arita, and C. Rosales-Guzmán, "Optical trapping with structured light: a review," *Adv. Photonics* **3**(3), 034001 (2021).
5. A. Marzo, M. Caleap, and B. W. Drinkwater, "Acoustic virtual vortices with tunable orbital angular momentum for trapping of Mie particles," *Phys. Rev. Lett.* **120**, 044301 (2018).
6. L. Yan, P. Gregg, E. Karimi, A. Rubano, L. Marrucci, R. Boyd, and S. Ramachandran, "Q-plate enabled spectrally diverse orbital-angular-momentum conversion for stimulated emission depletion microscopy," *Optica* **2**, 900-903 (2015).
7. C. Hnatovsky, V. G. Shvedov, W. Krolikowski, and A. V. Rode, "Materials processing with a tightly focused femtosecond laser vortex pulse," *Opt. Lett.* **35**(20), 3417-3419 (2010).
8. M. K. Sharma, J. Joseph, and P. Senthikumar, "Selective edge enhancement using anisotropic vortex filter," *Appl. Opt.* **50**(27), 5279-5286 (2011).
9. C. Xie, V. Jukna, C. Milián, R. Giust, I. Ouadghiri-Idrissi, T. Itina, J. M. Dudley, A. Couairon, and F. Courvoisier, "Tubular filamentation for laser material processing," *Sci. Rep.* **5**(1), 8914 (2015).
10. Z. Wang, N. Zhang, and X.-C. Yuan, "High-volume optical vortex multiplexing and de-multiplexing for free-space optical communication," *Opt. Express* **19**(2), 482–492 (2011).
11. Y. Yan, G. Xie, M. P. J. Lavery, H. Huang, N. Ahmed, C. Bao, Y. Ren, Y. Cao, L. Li, Z. Zhao, A. F. Molisch, M. Tur, M. J. Padgett, and A. E. Willner, "High-capacity millimetre-wave communications with orbital angular momentum multiplexing," *Nat. Commun.* **5**, 4876(2014).
12. G. Indebetouw, "Optical Vortices and Their Propagation," *J. Mod. Opt.* **40**(1), 73–87 (1993).
13. S. Orlov, K. Regelskis, V. Smilgevicius, and A. Stabinis, "Propagation of Bessel beams carrying optical vortices," *Opt. Commun.* **209**(1-3), 155–165 (2002).
14. H. T. Dai, Y. J. Liu, D. Luo, and X. W. Sun, "Propagation dynamics of an optical vortex imposed on an Airy beam," *Opt. Lett.* **35**(23), 4075–4077 (2010).
15. Y. Jiang, K. Huang, and X. Lu, "Propagation dynamics of abruptly autofocusing Airy beams with optical vortices," *Opt. Express* **20**(17), 18579–18584 (2012).
16. M. Born and E. Wolf, *Principles of Optics: Electromagnetic Theory of Propagation, Interference, and Diffraction of Light* (Pergamon Press, 1975).
17. I. Chremmos, P. Zhang, J. Prakash, N. K. Efremidis, D. N. Christodoulides, and Z. Chen, "Fourier-space generation of abruptly autofocusing beams and optical bottle beams," *Opt. Lett.* **36**(18), 3675–3677 (2011).
18. A. Zannotti, C. Denz, M. A. Alonso, and M. R. Dennis, "Shaping caustics into propagation-invariant light," *Nat. Communications* **11**, 3597 (2020).
19. S. N. Khonina, A. P. Porfirev, and A. V. Ustinov, "Sudden autofocusing of superlinear chirp beams," *J. Opt.* **20**, 025605 (2017).
20. V. A. Soifer, S. I. Kharitonov, S. N. Khonina, and S. G. Volotovskiy, "Caustics of vortex optical beams," *Dokl. Phys.* **64**, 276–279 (2019).
21. G. James, *Geometrical theory of diffraction for electromagnetic waves* (Peter Peregrinus Ltd., 1976).
22. B. R. Weinberg, *Asymptotic Methods in Equations of Mathematical Physics* (Gordon and Breach Science Publishers, 1989).
23. S. I. Kharitonov, S. N. Khonina, S. G. Volotovskiy, and N. L. Kazanskiy, "Caustics of the vortex beams generated by vortex lenses and vortex axicons," *JOSA A* **37** (3), 476-482 (2020).
24. M. V. Berry and K. T. McDonald, "Exact and geometrical optics energy trajectories in twisted beams," *J. Opt. A, Pure Appl. Opt.* **10**(3), 035005 (2008).
25. C. Xie, R. Giust, V. Jukna, L. Furfaro, M. Jacquot, P. A. Lacourt, L. Froehly, J. Dudley, A. Couairon, and F. Courvoisier, "Light trajectory in Bessel–Gauss vortex beams," *J. Opt. Soc. Am. A* **32**(7), 1313-1316 (2015).
26. M. Karpov, T. Congy, Y. Sivan, V. Fleurov, N. Pavloff, and S. Bar-Ad, "Spontaneously formed autofocusing caustics in a confined self-defocusing medium," *Optica* **2**, 1053-1057 (2015).

358 27. N. Xiao, C. Xie, E. Jia, J. Li, R. Giust, F. Courvoisier, and M. Hu, "Caustic Interpretation of the Abruptly
359 Autofocusing Vortex beams," *Opt. Express* **29**, 19975-19984 (2021).
360 28. A. H. Dorrah, M. Zamboni-Rached, and M. Mojahedi, "Frozen waves following arbitrary spiral and snake-like
361 trajectories in air," *Appl. Phys. Lett.* **110**(5), 051104 (2017).
362 29. I. D. Chremmos, Z. Chen, D. N. Christodoulides, and N. K. Efremidis, "Bessel-like optical beams with arbitrary
363 trajectories," *Opt. Lett.* **37**, 5003-5005 (2012).
364 30. J. Zhao, P. Zhang, D. Deng, J. Liu, Y. Gao, I. D. Chremmos, N. K. Efremidis, D. N. Christodoulides, and Z.
365 Chen, "Observation of self-accelerating Bessel-like optical beams along arbitrary trajectories," *Opt. Lett.* **38**,
366 498-500 (2013).
367 31. L. Froehly, F. Courvoisier, A. Mathis, M. Jacquot, L. Furfaro, R. Giust, P. A. Lacourt, and J. M. Dudley,
368 "Arbitrary accelerating micron-scale caustic beams in two and three dimensions," *Opt. Express* **19** (17), 16455-
369 16465 (2011).
370 32. M. Goutsoulas, D. Bongiovanni, D. Li, Z. Chen, and N. K. Efremidis, "Tunable self-similar Bessel-like beams
371 of arbitrary order," *Opt. Lett.* **45**, 1830-1833 (2020).
372 33. I. A. Litvin, T. Mhlanga, and A. Forbes, "Digital generation of shape-invariant Bessel-like beams," *Opt.*
373 *Express* **23**(6), 7312-7319 (2015).
374 34. S. N. Khonina, S. I. Kharitonov, S. G. Volotovskiy and V. A. Soifer, "Caustics of non-paraxial perfect optical
375 vortices generated by toroidal vortex lenses", *Photonics* **8**(7), 259 (2021).
376 35. J. W. Goodman, *Introduction to Fourier Optics 2nd Ed* (McGraw-Hill, 1996).
377 36. L. J. Wong, D. N. Christodoulides, and I. Kaminer, "The complex charge paradigm: A new approach for
378 designing electromagnetic wavepackets," *Adv. Sci.* **7**(19), 1903377 (2020).
379 37. L. J. Wong, "Propagation-invariant space-time caustics of light," *Opt. Express* **29**(19), 30682-30693 (2021).